Astroparticle Physics 97 (2018) 19–26

Contents lists available at ScienceDirect

Astroparticle Physics

journal homepage: www.elsevier.com/locate/astropartphys

# Actuation crosstalk in free-falling systems: Torsion pendulum results for the engineering model of the LISA pathfinder gravitational reference sensor

M. Bassan[a,b], A. Cavalleri[c], M. De Laurentis[d,e], F. De Marchi[f], R. De Rosa[d,e], L. Di Fiore[e,*], R. Dolesi[c], N. Finetti[g,h], F. Garufi[d,e], A. Grado[i,e], M. Hueller[c], L. Marconi[j], L. Milano[d,e], Y. Minenkov[b], G. Pucacco[a,b], R. Stanga[k,h], D. Vetrugno[c], M. Visco[l,b], S. Vitale[c], W.J. Weber[c]

[a] Dipartimento di Fisica, Università di Roma "Tor Vergata", I-00133 Roma, Italy
[b] INFN - Sezione di Roma Tor Vergata, I-00133 Roma, Italy
[c] Dipartimento di Fisica, Università di Trento and INFN - TIFPA, I-38050 Povo (TN), Italy
[d] Dipartimento di Fisica, Università di Napoli "Federico II", I-80126, Napoli, Italy
[e] INFN - Sezione di Napoli, I-80126, Napoli, Italy
[f] Dipartimento di Ingegneria Meccanica e Aerospaziale, DIMA, Sapienza, Università di Roma - 00184 Roma, Italy
[g] Dipartimento di Scienze Fisiche e Chimiche, Università degli Studi dell'Aquila, I-67100 l'Aquila, Italy
[h] INFN - Sezione di Firenze, I-50019 Firenze, Italy
[i] INAF - Osservatorio Astronomico di Capodimonte, I-80126 Napoli, Italy
[j] Istituto Nazionale di Ottica - CNR - 50125 Firenze, Italy
[k] Dipartimento di Fisica ed Astronomia, Università degli Studi di Firenze, I-50019 Firenze, Italy
[l] INAF - Istituto di Astrofisica e Planetologia Spaziali, I-00133 Roma, Italy

ARTICLE INFO

*Article history:*
Received 10 March 2017
Revised 20 October 2017
Accepted 21 October 2017
Available online 26 October 2017

*Keywords:*
Inertial motion
Crosstalk
Torsion pendulum
LISA
Actuation

ABSTRACT

In this paper we report on measurements on actuation crosstalk, relevant to the gravitational reference sensors for LISA Pathfinder and LISA. In these sensors, a Test Mass (TM) falls freely within a system of electrodes used for readout and control. These measurements were carried out on ground with a double torsion pendulum that allowed us to estimate both the torque injected into the sensor when a control force is applied and, conversely, the force leaking into the translational degree of freedom due to the applied torque.

The values measured on our apparatus (the engineering model of the LISA Pathfinder sensor) agree to within 0.2% (over a maximum measured crosstalk of 1%) with predictions of a mathematical model when measuring force to torque crosstalk, while it is somewhat larger than expected (up to 3.5%) when measuring torque to force crosstalk. However, the values in the relevant range, i.e. when the TM is well centered ($\pm 10\,\mu$m) in the sensor, remain smaller than 0.2%, satisfying the LISA Pathfinder requirements.



## 1. Introduction

Torsion pendulums [1] are the instruments of choice to approach, in an Earth-based laboratory, the conditions of free fall: this is because one degree of freedom (DoF) of the pendulum, the rotation around the suspension fiber, experiences an extremely small restoring force (better, torque) from the fiber: in pendulum jargon, this is usually called the *soft*, i.e. almost free, DoF. This is particularly important for studies that lead to the realization of space experiments requiring Test Masses (TMs) in geodesic motion, like the gravitational wave observatory LISA [2]. We developed a double pendulum with two soft degrees of freedom [3]. This pendulum, nicknamed PETER (acronym for PEndulum free in Translation and Rotation), is a facility devoted to characterizing, using its two soft degrees of freedom, some features of the LISA Pathfinder (LPF)[4,5] electrostatic readout that could not be tested on simple pendulums: namely, the crosstalk in sensing and actuation, the orthogonality of feedback signals and other residual interactions between the TM and its environment. In the LPF mission it is crucial to properly evaluate the amount of crosstalk that control signals feed into one DoF while acting on the other. While the sensing

* Correspondig author.
*E-mail address:* difiore@na.infn.it (L. Di Fiore).

https://doi.org/10.1016/j.astropartphys.2017.10.010
0927-6505/

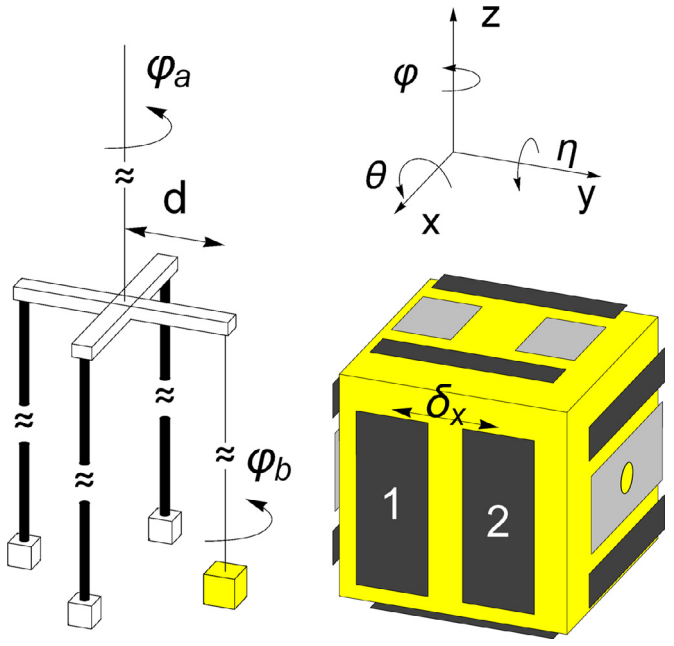


**Fig. 1.** A sketch of the PETER pendulum, with the two torsion fibers in cascade. $\varphi = \varphi_a + \varphi_b$ and $x = d \cdot \varphi_a$ are the coordinates of the two soft DoFs. A diagram of the GRS electrodes, surrounding the TM, is also shown: the gray electrodes feed a.c. bias while the black ones are for sensing and actuation. Labels 1 and 2 indicate two of the four electrodes sensing $x$ and $\varphi$ DOFs: each one is paired in a bridge with an identical electrode on the opposite side (call them 3 and 4). By applying an electric field to electrodes 1 and 2 we can actuate a force along $x$ on the TM, while electrodes 1 and 4 would be used to apply a torque on $\varphi$.

crosstalk is negligible, because LPF uses an interferometric readout with superior performance, the crosstalk in actuation could indeed be a limiting factor to the sensitivity: the electrostatic actuation keeps the TMs in position along the non-critical DOFs, and therefore is continuously active during operations.

The PETER pendulum was used to investigate crosstalk issues before the launch of LPF and has been kept operational in the Gravitation Physics Laboratory in Napoli, as a ground support equipment during mission data taking.

The apparatus was described in previous papers [3,6]; we just recall here that two soft DoFs are obtained, as shown in the sketch of Fig. 1, by suspending the test mass (a hollow, 46 mm, gold coated Al cube) on a cascade of two fibers: on the top, a 100 µm Tungsten fiber suspends a crossbar (oscillation period 765.1 s); anchored at one end of the crossbar, a second fiber (25 µm diameter), made of the same material, suspends the TM (oscillation period 487.2 s), that hangs inside the electrostatic readout case. The lower fiber provides an almost free rotation around the $z$ axis, that coincides with the fiber itself, while the top fiber allows a soft motion along a $d = 150$ mm (the length of the crossbar arm) radius arc: for most practical purposes this motion can be assumed as a translation. The two soft DoFs are then the rotation angle $\varphi$ and the translation along the $x$ axis. Motion in all six DoFs is measured by the Electrode Housing (EH), a set of electrodes that provide electrostatic readout and actuation, described below. This system, i.e. the TM, the EH, and the sensor electronics, constitute the so called Gravitational Reference Sensor (GRS) [7]. For redundancy, better sensitivity and cross check, the soft DoFs are also monitored by two optical lever readouts [9,10] measuring the rotation $\varphi_a$ of the crossbar and the position $x$ and rotation $\varphi$ of a mirror attached to the shaft suspending the TM.

The two soft DoFs are read (and actuated) by the same 4 electrodes, although in different configuration, as shown in Fig. 1: by applying an electric field to two adjacent electrodes (1 and 2 in Fig. 1) we apply a force to the TM. Conversely, an electric field applied to two electrodes diagonally across the TM will produce a torque. This constitutes a source of crosstalk between the DoFs, that we aim to investigate.

Here we report the results of measurement campaigns, performed before the launch of LPF, devoted to evaluating the crosstalk in actuation.

In Section 2 we describe the measurement technique, in Section 3 we describe force to torque crosstalk ($CT_{F\to\tau}$) measurements performed by applying a force on the suspended pendulum mass and measuring the corresponding (unwanted) torque. Torque to force crosstalk ($CT_{\tau\to F}$) measurements were also performed in similar way and are reported in Section 4.

## 2. Methods and goals of the investigation

The main goal of the measurements reported here is to evaluate the actuation crosstalks of the GRS. The TM (that in space experiments is freely floating, while in our Earth based apparatus is suspended by torsion fibers) is surrounded by the EH, a hollow metal box padded with 18 electrodes facing each side of the TM (see Fig. 1). Six of these are used to provide a.c. bias, while the other 12, two per side, are arranged in 6 capacitive bridges and permit to monitor the motion of the TM along all its translational and rotational DOFs. The same electrodes can be individually biased with control voltages in order to apply forces or torques.

The requirement for LPF actuation crosstalk [8] are only defined for force induced along the interferometer axis $x$, by actuation on the other 5 DOFs (i.e. force along $y$ and $z$ and torques around the three axes). For the force to force terms (that cannot be tested with our apparatus), the specification is to stay within 0.1% in crosstalk. For torque around the $\theta$ and $\eta$ axes the specification is, in our notation, described below in Eq. (1), 0.23%, while requirement for torque around the $\varphi$ axis is 0.67%. The latter is the only one that we can directly test. All the crosstalks on other DOFs do not have specifications because they cannot contribute significantly to the LPF (and LISA) noise budget [8].

The EH (we use the LPF *engineering model*) can be remotely moved in 5 degrees of freedom by motorized micro-positioners; additionally, the suspension point of the top fiber can be raised and rotated: this allows us to align the TM at the center of the EH, and parallel to its walls. We remark here that the geometrical zero, the position where the TM appears to be properly centered in the EH, with equally wide gap pairs on each direction, does not necessarily coincide, in real life, with electrical zero of the GRS, i.e. the TM position where all capacitive bridges measuring its position are zeroed. This can be due to imperfections of both electrical (capacitances not properly balanced) and mechanical origin. Transduction and actuation is operated by a read-out and control electronics unit, specially developed by ETH-Zürich [11]. We aim to evaluate the actuation cross couplings as a function of the relative position between EH and TM and verify to what extent they agree with the values predicted by a simple electrostatic model.

The crosstalks are defined as

$$CT_{F\to\tau} = \frac{\tau_m}{F_a \cdot \delta_x} \qquad CT_{\tau\to F} = \frac{F_m \cdot \delta_x}{\tau_a} \tag{1}$$

Where the subscripts $a$, $m$ refer to *a*ctuating or measured quantities and $\delta_x = 21.5$ mm, the distance between the center of two adjacent x electrodes, is the natural length scale to convert force into torque. We remark that, in all cases, we apply voltages to the EH electrodes, and measure both the resulting force and the resulting torque. The crosstalks of Eq. (1) are therefore estimated as ratios of measured dynamic quantities.

An analytical expression for the crosstalks can be found by taking into account electrode geometry and TM-EH relative position

on the three DOFs that experience large motion during our measurements: $x$, $y$ and $\varphi$. Details about this model can be found in Appendix A. The resulting expressions for the crosstalks are:

$$CT_{F\to\tau} = \left(\frac{3\delta_x}{2h_x^2} + \frac{s}{\delta_x h_x} + \frac{1}{2\delta_x}\right)x\varphi + \frac{y}{\delta_x} \tag{2}$$

$$CT_{\tau\to F} = \frac{6\delta_x}{h_x^2}x\varphi \tag{3}$$

where $h_x = 4$ mm is the gap between the TM and the GRS along the $x$-axis, and $s = 46$ mm is the side of the TM. Both the electrodes and the TM are assumed ideal: imperfections, asymmetries, border effects and finite size of the TM are neglected

The measurements are performed by actuating with a sinusoidal force (or torque) on the TM and reading its displacement $x$ and rotation $\varphi$; each measurement must last many periods of the pendulum oscillations, in our case a few hours. The force ($F$) and the torque ($\tau$) acting on the TM are then estimated from $x$ and $\varphi$, through the equations of the pendulum dynamics, as described in [3]. In order to evaluate the dependence of crosstalk on the relative TM-EH position, the EH is moved with micro-positioners along the horizontal $(x-y)$ plane, in selected positions on a regular pattern, as can be seen in Figs. 3 and 5, and the procedure is repeated for each position.

Calibration of the apparatus requires a few steps; we remind that force and torque are computed solving the equations of motion of the system, where displacement and rotation ($x$, $\varphi$) are the independent variables and the mechanical properties of the pendulums appear as coefficients [3]. As a first step, direct calibration of position and angle readings was obtained by moving the EH, with motorized precision stages, around the TM (rigidly held on the bench) and comparing the GRS readings with the nominal reading of the stage encoder.

This calibration was independently checked with a high precision touch probe and is accurate to better than 1%. Then, the mechanical parameters of the two pendulums were evaluated as follows: the elastic constants of both fibers were independently measured (within 1–2%) on an ad-hoc facility, by hanging various discs of known moment of inertia and measuring the oscillation periods. Once the fiber constants are known, the moments of inertia of TM and crossbar were derived by fitting the 8 lowest resonances of PETER (measured to better than 1%), to an accurate analytical model in 8 degrees of freedom [12]. Finally, force and torque are derived (with an accuracy of about 2%) from GRS readout by solving the equation of motion with the measured mechanical parameters.

The data are affected by a readout crosstalk, due to a geometrical effect: the measured position of $x$ also depends on the coordinates $\varphi$ and $y$, according to:

$$x = x_{GRS} - (y_{GRS} - y_c)\cdot\varphi \tag{4}$$

where $x_{GRS}$, $y_{GRS}$ and $\varphi$ are the calibrated signals as read by the GRS and $y_c$ is the distance, along $y$, from the geometrical center of the TM of the vertical axis of rotation ; $y_c$ differs from zero if the suspending wire and the shaft connecting it to the TM are not perfectly aligned. As a consequence, the center of mass (that, by definition, lies on the vertical rotation axis) does not coincide with the geometrical center of the TM. This is illustrated in Fig. 2, where the effect was largely exaggerated. Other effects due to TM asymmetries can be found in [13].

The data were corrected according to Eq. (4), using the value $y_c = 23 \pm 5\,\mu$m estimated by fitting the data. Neglecting this correction would result in largely overestimating the crosstalks. This effect, relevant to suspended masses as in our case, does not show up in free-falling TMs, as long as the center of mass coincides with the geometrical center. Similar corrections could also be considered for the other DOFs, but they are not relevant for our measurements.

**Table 1**
Relevant information for the six measurement runs. Run 3b was performed in constant stiffness conditions.

| Run | Run start date | Avg. time per step (h) | Number of steps | Step size (μm) | Actuation ampl. ($V^2$) |
|---|---|---|---|---|---|
| Force to Torque crosstalk (actuation force at 14 mHz) | | | | | |
| 1a | Jun 9, 2015 | 3 | 5×5 | 100 | 50 |
| 2a | Jun 19, 2015 | 1.25 | 37 (spiral) | 100 | 20 |
| 3a | Jun 26, 2015 | 2 | 24 (spiral) | 100 | 20 |
| Torque to Force crosstalk (actuation torque at 18 mHz) | | | | | |
| 1b | May 25, 2015 | 3 | 8 | 150 | 20 |
| 2b | May 29, 2015 | 3 | 24 | 100 | 20 |
| 3b | No. 24, 2015 | 2 | 8 (spiral) | 100 | 20 |

**Table 2**
Coefficients for the quadratic polynomial in the three variables x,y,$\varphi$ that best fits the $CT_{F\to\tau}$ data of all 3 runs. The last column shows the crosstalk one derives, based on this fit, at the edge of the relevant, central region of operation: 10 μm away from the center in both x and y, and 100 μrad tilt in $\varphi$. Note that the crosstalk units, for consistency with the rest of the paper, are percent: e.g., the largest value of the last column reads 0.046%, that is $4.6\cdot10^{-4}$. In the worst case scenario, where we sum the absolute value of all the contributions, we have a total crosstalk of 0.053%, and therefore still negligible.

| polynomial terms | units | analytical model | fitted coefficients | $CT_{F\to\tau}$ (%) at edge |
|---|---|---|---|---|
| $x^2$ | $\mu m^{-2}$ | 0 | $(-1.9\pm0.8)\cdot10^{-7}$ | $-1.9\cdot10^{-5}$ |
| $y^2$ | $\mu m^{-2}$ | 0 | $(-1.8\pm0.5)\cdot10^{-7}$ | $-1.8\cdot10^{-5}$ |
| $\varphi^2$ | - | 0 | $(-6.3\pm5)\cdot10^{-9}$ | $-6.4\cdot10^{-5}$ |
| x y | $\mu m^{-2}$ | 0 | $(9.3\pm6)\cdot10^{-8}$ | $9.3\cdot10^{-6}$ |
| $x\varphi$ | $\mu m^{-1}$ | $2.5\cdot10^{-7}$ | $(3.2\pm0.4)\cdot10^{-7}$ | $3.2\cdot10^{-4}$ |
| $y\varphi$ | $\mu m^{-1}$ | 0 | $(1.7\pm2)\cdot10^{-8}$ | $1.7\cdot10^{-5}$ |
| x | $\mu m^{-1}$ | 0 | $(-5.4\pm0.3)\cdot10^{-4}$ | $-0.0054$ |
| y | $\mu m^{-1}$ | $4.65\cdot10^{-3}$ | $(4.56\pm0.01)\cdot10^{-3}$ | 0.0456 |
| $\varphi$ | - | 0 | $(-9\pm7)\cdot10^{-6}$ | $-8.9\cdot10^{-4}$ |
| - | - | 0 | $(0\pm2)\cdot10^{-3}$ | $-9.6\cdot10^{-5}$ |

We report here on six measurement runs, summarized in Table 1: three to evaluate the force to torque crosstalk, i.e. $CT_{F\to\tau}$, and three for $CT_{\tau\to F}$.

## 3. Force to torque crosstalk

In Fig. 3 the results of the measurement run 3a, compared to the predictions of the analytical model, are reported, together with the relative residuals (measured values minus model predictions) vs. $x$ displacement. The general agreement is good with a residual small discrepancy, well represented by a linear trend along $x$.

In Fig. 4 the results of the runs 1a, 2a and 3a are compared. Although the measurements were performed in different conditions (see Table 1), the $CT_{F\to\tau}$ are very repeatable. We fitted with a second order surface in $x$, $y$ and $\varphi$ the measurement points of the three runs. The residuals of all the runs with respect to this surface are within less than 0.035%. In all the runs the maximum observed crosstalk is $\pm1\%$ in the whole high resolution range of the GRS ($\pm200$ μm), with a disagreement below 0.2% with respect to the model predictions. This residual disagreement can be due either to some (geometrical and/or electronic) asymmetry in our GRS or to some inaccuracy in the knowledge of the mechanical parameters.

In Table 2 we report the coefficients of the polynomial fitting the data, compared to those predicted by the analytical model. This parametrization allows us to compute the expected crosstalk at any TM position inside the EH. In order to enhance the relevance of the various terms, the last column of Table 2 shows the contribution of each single term of the polynomial to the total crosstalk, computed

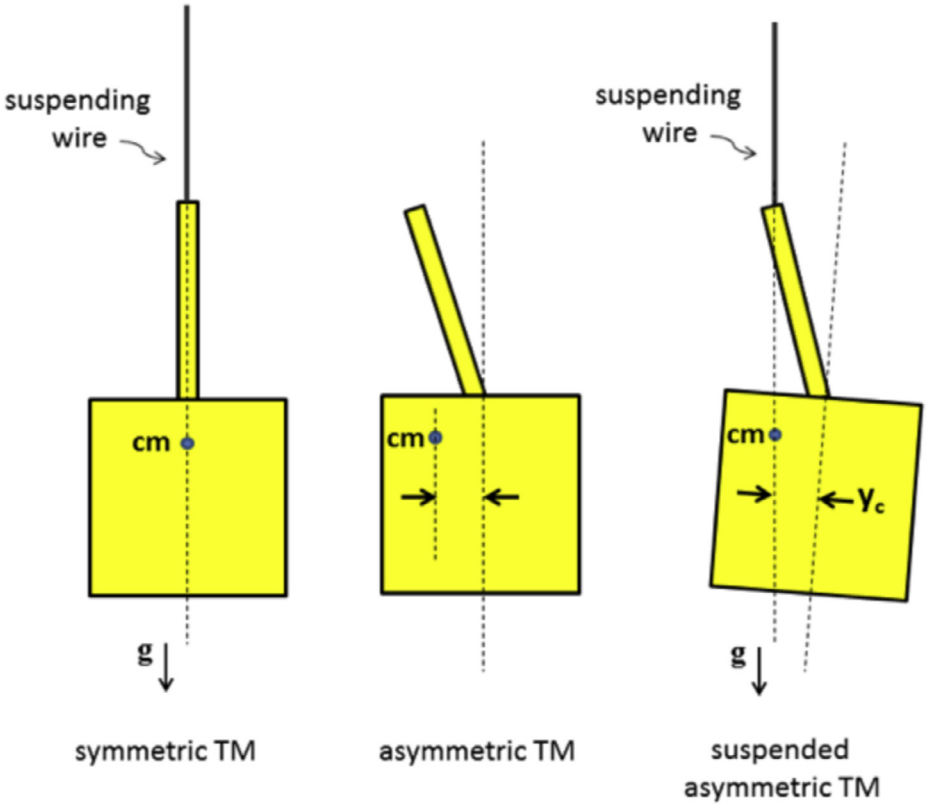


**Fig. 2.** Displacement of vertical rotation axis with respect to TM geometric center, due to TM-shaft asymmetry. Note that the EH is aligned to the cube faces, not to the vertical direction.

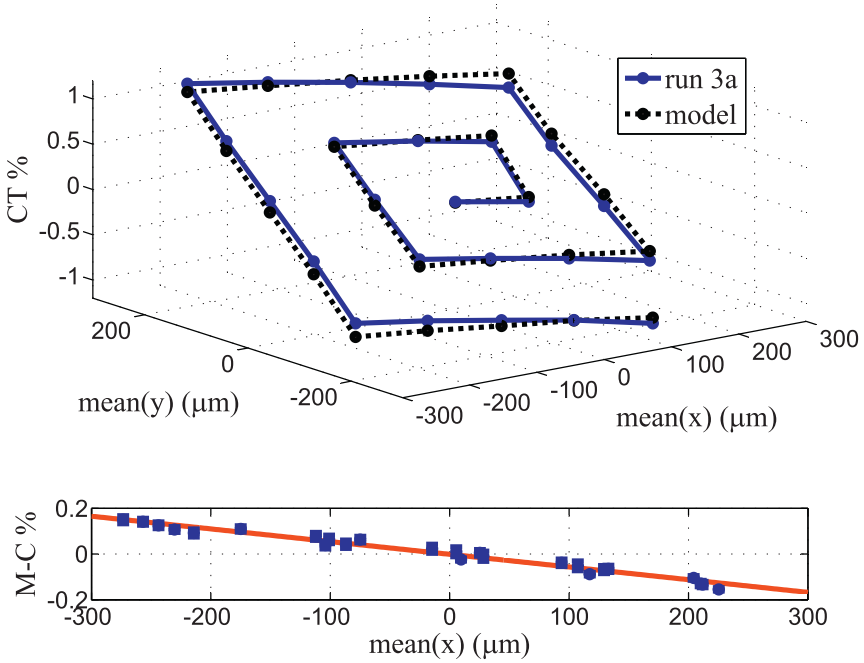


**Fig. 3.** Crosstalk $CT_{F\to\tau}$ as defined in Eq. (1), for the run 3a, compared to the analytical model of Eq. (2). In the lower part of the figure the M-C residuals (Measured minus Computed) are shown versus the x coordinate. As we can see, there is a small discrepancy, well represented by a linear fit.

at one edge of the measurement range of interest for the scientific operations of LPF ($x = y = 10\,\mu$m, $\varphi = 100$ μrad). In order to estimate a worst case scenario in this range, we can sum the absolute value of all the contributions, obtaining a total crosstalk of 0.053%, that is negligible.

## 4. Torque to force crosstalk

In Fig. 5 the results of the measurement run 2b are shown and compared with the analytical model. The relative residuals (M-C) are also shown vs. $x$ displacement. Unlike the previous case, we have here a much larger disagreement with the model; however,

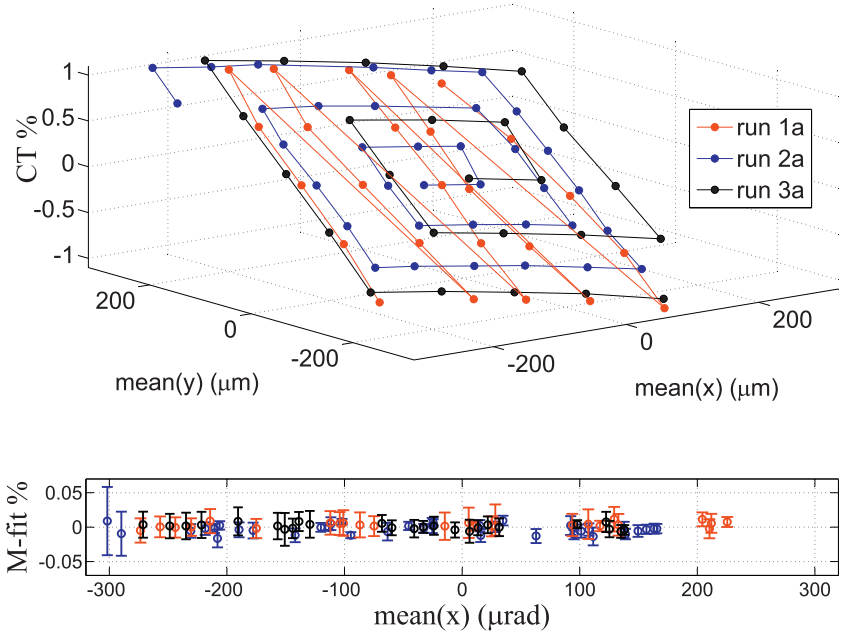


**Fig. 4.** $CT_{F\to\tau}$ measured in the three different runs 1a, 2a and 3a. The residuals shown in the lower frame are calculated with respect to a second order fit surface to the points of the three runs.

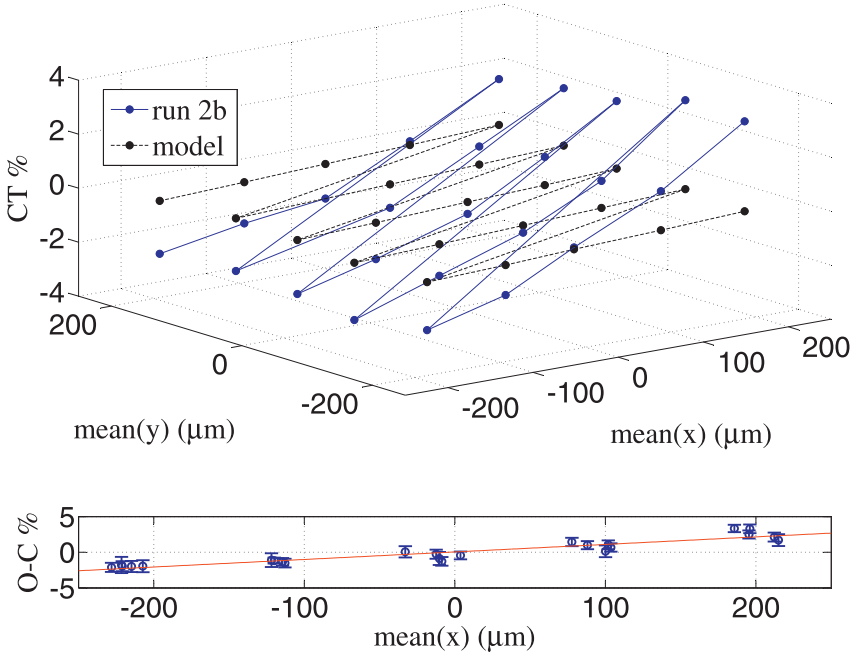


**Fig. 5.** Measured $CT_{\tau\to F}$ compared with the model. In the lower frame the residuals (M-C), seen on a constant $y$ cross section.

also in this instance, the dominant effect exhibits a linear trend in the residuals, presently under investigation.

In Fig. 6 the results of the runs 1b, 2b and 3b are compared. The measured torque to force crosstalks are well repeatable. Also in this case, we fitted with a second order surface in $x$, $y$ and $\varphi$ the measurement points of the three runs. The residuals of all the runs with respect to this surface, shown in the lower frame, are compatible with zero within the measurement error.

It can be seen in these plots that the measured values of $CT_{\tau\to F}$ reach values as large as 3.5% at the limit of the High Resolution (HR) range ($\pm 200\,\mu m$) of the front-end electronics and are larger, by an order of magnitude, than expected. Nevertheless, the level of $CT_{\tau\to F}$ falls below 0.8% in the central $\pm 50\,\mu m$ and is less than 0.2% at the GRS center.

In order to verify if the disagreement was due to the actuation modality, run 3b was performed in *constant stiffness* conditions [14] where the net TM actuation force is a sum of opposing forces applied from both sides of the TM while maintaining the sum of the force magnitudes constant, which maintains a constant force gradient. No difference was observed, as expected.

In Table 3, the coefficients of the polynomial fitting the data are reported as described in Section 3. In this case, we obtain a worst case total crosstalk of 0.18%, larger than in the case of $CT_{F\to\tau}$ but still compliant with the GRS specifications.

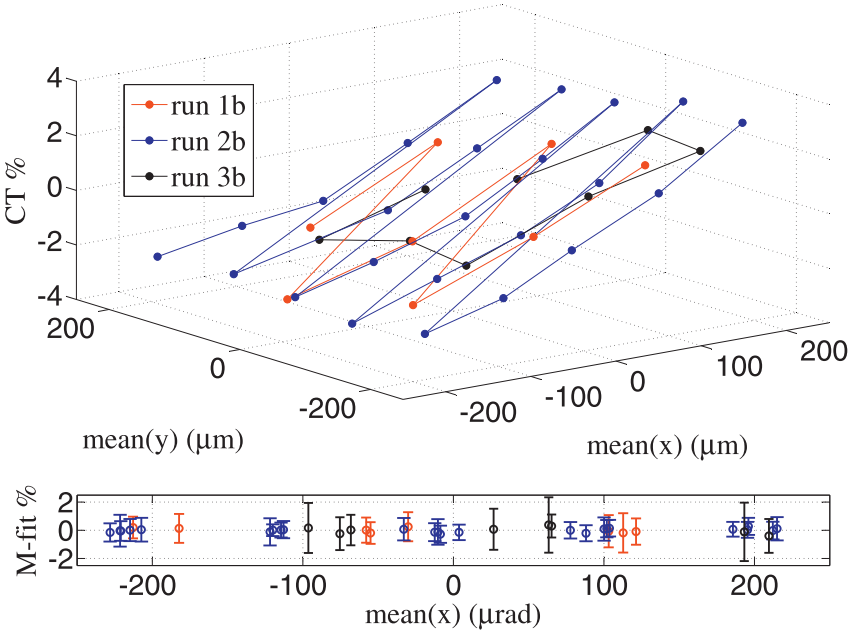


**Fig. 6.** $CT_{\tau\to F}$ measured in the three different runs 1b, 2b and 3b. The residuals shown in the lower frame versus the $x$ coordinate, are calculated with respect to a second order fit surface to the points of the three runs.

**Table 3**
Torque to Force crosstalk: coefficients of the best fit quadratic polynomial in x,y,$\varphi$. See caption of Table 2 for details. In the worst case scenario, where we sum the absolute value of all the contributions, we have a total crosstalk of 0.18%.

| polynomial terms | units | analytical model | fitted coefficients | $CT_{\tau\to F}$ (%) at edge |
|---|---|---|---|---|
| $x^2$ | $\mu m^{-2}$ | 0 | $(1.5\pm3)\cdot10^{-6}$ | $1.5\cdot10^{-4}$ |
| $y^2$ | $\mu m^{-2}$ | 0 | $(-9\pm4)\cdot10^{-6}$ | $-9\cdot10^{-4}$ |
| $\varphi^2$ | - | 0 | $(5\pm5)\cdot10^{-7}$ | 0.005 |
| $xy$ | $\mu m^{-2}$ | 0 | $(1.3\pm0.4)\cdot10^{-6}$ | 0.0013 |
| $x\varphi$ | $\mu m^{-1}$ | $4.0\cdot10^{-7}$ | $(4\pm2)\cdot10^{-6}$ | 0.0036 |
| $y\varphi$ | $\mu m^{-1}$ | 0 | $(-2\pm2)\cdot10^{-6}$ | −0.0016 |
| $x$ | $\mu m^{-1}$ | 0 | $(7\pm2)\cdot10^{-3}$ | 0.069 |
| $y$ | $\mu m^{-1}$ | 0 | $(-1\pm2)\cdot10^{-3}$ | −0.02 |
| $\varphi$ | - | 0 | $(1\pm1)\cdot10^{-3}$ | −0.088 |
| | - | 0 | $(0\pm0.5)$ | 0 |

## Conclusions

We reported the on-ground evaluation of the actuation crosstalk for the electrostatic actuators of the LPF Test Mass. We have measured the crosstalk from force to torque, $CT_{F\to\tau}$, expressed as the amount of unwanted detected torque, generating a residual $\varphi$ rotation, when a force is applied to the TM. Analogously, we measured the crosstalk from torque to force $CT_{\tau\to F}$, by applying a torque to the TM and measuring the resulting force along $x$, generating linear motion. This is a potential noise source for the relative acceleration of the TMs in space. In our analysis, we have removed an undue readout crosstalk, generated by an offset of the TM center of mass with respect to the suspension axis, evaluated in 23 ± 5 μm.

The measurements of $CT_{F\to\tau}$ turn out to be very close to the model predictions, while, in the characterization of $CT_{\tau\to F}$, our data show measured values larger than expected, up to 3.5% in the outermost region of the EH. In order to verify if this disagreement can be explained by manufacturing imperfections, we would need a more sophisticated model taking in account electrode and TM asymmetries. This will be considered in following studies for LISA, but is beyond the scope of this paper.

However, the results of our investigations show that, when the TM is well centered, i.e. in the region (±10 μm in $x$ and $y$, ±100 μrad in $\varphi$) of the GRS where operations in space take place, $CT_{\tau\to F}$ is well below 0.23%, that is the most stringent requirement given for torque to force crosstalk.

In conclusion, the measurements confirm that in the engineering model GRS for LISA Pathfinder the actuation crosstalks are in agreement with the expectations and with the specifications for LPF and LISA.

## Appendix A. Actuation model for the LPF inertial sensor

The following model is based mainly on [15]. The capacitance formed by each electrode $EL_i$ and the TM can be computed, using the infinite plane approximation, in the case of rectangular electrodes with sides $l_x$ and $w_x$ along $Z$ and $Y$ axis respectively (see Fig. A.7), by:

$$C_i = \varepsilon_0 \int_{-l_x/2}^{l_x/2} \int_{y_i-w_x/2}^{y_i+w_x/2} \frac{1}{d} \mathrm{d}Z\mathrm{d}Y \tag{A.1}$$

where $d$ is the distance between $P(X, Y)$ and the TM, $y_i$ is the $EL_i$ center coordinate along $Y$ axis. Since the TM is displaced from its nominal position by $(x, y)$ and rotated by the angle $\varphi$, the distance $d$ is not a constant value, as in the parallel electrodes case, but depends on TM translations and rotations. By focusing the analysis on the electrode number 2, the distance $d$ is simply $d = \varphi(Y - Y_0)$ , where $Y_0$ is the $Y$ coordinate of the intersection point of the lines of equation (see Fig. A.7):

$$X = \frac{s}{2} + h_x; \quad X = -Y\tan\varphi + y + x\tan\varphi + \frac{1}{2}s\sec\varphi$$

and $Y$ is the second coordinate of the electrode point $P$. In this way, for the $EL_2$, the integral (A.1) yields:

$$C_2 = C_0 \frac{h_x}{w_x\varphi} \ln\left[1 + \frac{w_x\tan\varphi}{h_x - x + (\frac{\delta_x}{2} - \frac{w_x}{2} - y)\tan\varphi + \frac{s}{2}\frac{\cos\varphi - 1}{\cos\varphi}}\right]$$

where

$$C_0 = \varepsilon_0 \frac{l_x w_x}{h_x}$$

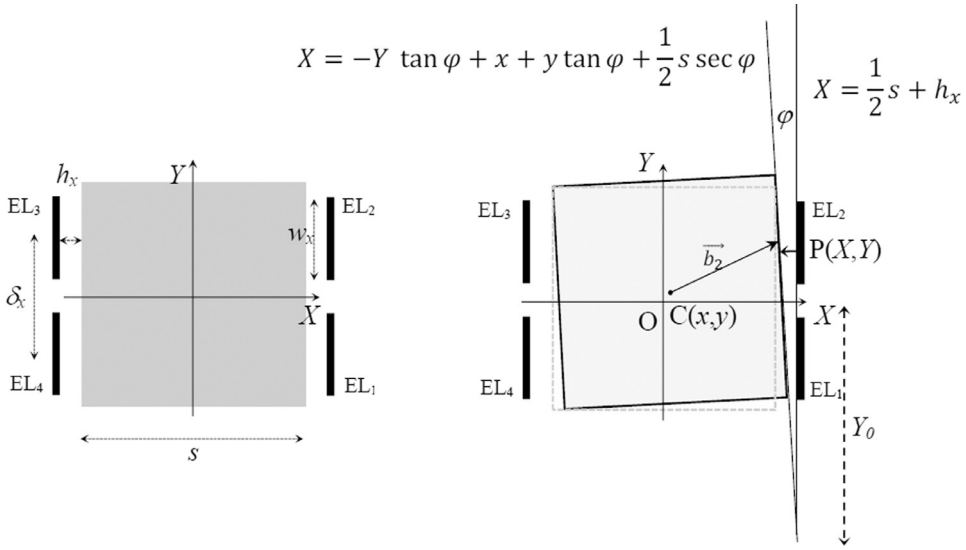


**Fig. A1.** Test Mass with the *X* electrodes in nominal and roto-translated position (top view).

is the *nominal* (i.e. centered and un-tilted TM) capacitance. Similar expressions can be found for the other capacitors. Forces and torques on the TM can be obtained by suitable combinations of electrode polarizations. The control electronics provides four actuation polarizations: $V_{x1}$ applied on electrodes $EL_1$, $EL_2$, $V_{x2}$ applied on electrodes $EL_3$, $EL_4$, $V_{\varphi 1}$ applied on electrodes $EL_1$, $EL_3$, $V_{\varphi 2}$ applied on electrodes $EL_2$, $EL_4$.

By focusing on sinusoidal actuations of amplitude $A_F$ for the force and $A_\tau$ for the torque, and angular frequency $\omega$, to actuate a force or a torque, the polarizing voltages should be, respectively:

$$V_{x1} = \begin{cases} \sqrt{A_F \sin\omega t} & \sin\omega t \geq 0 \\ 0 & \sin\omega t < 0 \end{cases};\quad V_{x2} = \begin{cases} 0 & \sin\omega t \geq 0 \\ \sqrt{-A_F \sin\omega t} & \sin\omega t < 0 \end{cases} \tag{A.2}$$

$$V_{\varphi 1} = \begin{cases} \sqrt{A_\tau \sin\omega t} & \sin\omega t \geq 0 \\ 0 & \sin\omega t < 0 \end{cases};\quad V_{\varphi 2} = \begin{cases} 0 & \sin\omega t \geq 0 \\ \sqrt{-A_\tau \sin\omega t} & \sin\omega t < 0 \end{cases} \tag{A.3}$$

By neglecting the TM voltage, the electrostatic actions given by all the other electrodes, and taking into account only actuations in the (*X*, *Y*) plane, i.e. forces along *X* and *Y* ($F_x$, $F_y$) and torque along *Z* ($\tau$), we obtain:

$$F_x = \frac{1}{2}\sum_{i=1}^{4}\frac{\partial C_i}{\partial x}V_i^2;\quad F_y = \frac{1}{2}\sum_{i=1}^{4}\frac{\partial C_i}{\partial y}V_i^2;\quad \tau = \frac{1}{2}\sum_{i=1}^{4}M_i V_i^2 \tag{A.4}$$

where $M_i$ is the *Z* component of $(\mathbf{b}_i \wedge \nabla C_i)$ and $\mathbf{b}_i$ is the vector from the TM center $C(x, y)$ to the projection of the center of the electrode $EL_i$ on the corresponding TM surface (see Fig. A.7).

Even if only one actuation type is commanded, the polarization of the $EL_i$ electrode always produces actuation in both force and torque. Indeed, putting together Eqs. (A.2), (A.3), and (A.4) one get:

$$F_x(t) = \begin{cases} \frac{1}{2}[(C_{1,x}+C_{2,x})A_F + (C_{1,x}+C_{3,x})A_\tau]\sin\omega t & \sin\omega t \geq 0 \\ -\frac{1}{2}[(C_{3,x}+C_{4,x})A_F + (C_{2,x}+C_{4,x})A_\tau]\sin\omega t & \sin\omega t < 0 \end{cases}$$

$$\tau(t) = \begin{cases} \frac{1}{2}[(M_1+M_3)A_\tau + (M_1+M_2)A_F]\sin\omega t & \sin\omega t \geq 0 \\ -\frac{1}{2}[(M_2+M_4)A_\tau + (M_3+M_4)A_F]\sin\omega t & \sin\omega t < 0 \end{cases}$$

where $C_{i,x} = dC_i/dx$.

It is worth noting that mixed terms that arise when squaring the voltage expression of Eqs. (A.4) give no contribution since the driving electronics modulate each actuation voltage at a different frequency for the two different actuations. For the following analysis we need to find the amplitude of the fundamental harmonic of the actuations $F_x$ and $\tau$. Their amplitudes can be easily found by computing the corresponding Fourier components, and are:

$$F_\omega = \frac{1}{2}A_F(C_{1,x}+C_{2,x}-C_{3,x}-C_{4,x}) + \frac{1}{2}A_\tau(C_{1,x}+C_{3,x}-C_{2,x}-C_{4,x})$$
$$\tau_\omega = \frac{1}{2}A_\tau(M_1+M_3-M_2-M_4) + \frac{1}{2}A_F(M_1+M_2-M_3-M_4)$$

To proceed further, the expressions of $C_{i,x}$ and $M_i$ are needed. The full expressions are cumbersome and not very useful. Since the expected displacements and rotation are very small, it is more convenient to use approximate expressions. By truncating to the second order in *x*, *y* and $\varphi$ it results, for example:

$$C_{1,x} = \frac{C_0}{h_x}\left(1 + \frac{2}{h_x}x + \frac{\delta_x}{h_x}\varphi + \frac{3\delta_x}{h_x^2}x\varphi + \frac{2}{h_x}y\varphi + \frac{3}{h_x^2}x^2 + K_1\varphi^2\right)$$
$$M_1 = \frac{C_0\delta_x}{2h_x}\left(1 + \frac{2}{h_x}x + \frac{2}{\delta_x}y + K_2\varphi + \frac{3}{h_x^2}x^2 + \frac{4}{h_x\delta_X}xy + \frac{4}{h_x}y\varphi + K_3x\varphi + K_4\varphi^2\right)$$

and similar expressions for the other coefficients, being:

$$K_1 = \frac{1}{3} + \frac{s}{2h_x} + \frac{w_x^2}{4h_x^2} + \frac{3\delta_x^2}{4h_x^2} \qquad K_2 = \frac{\delta_x}{h_x} + \frac{h_x}{\delta_x} + \frac{s}{\delta_x}$$
$$K_3 = \frac{2s}{h_x\delta_x} + \frac{3\delta_x}{h_x^2} + \frac{1}{\delta_x} \qquad K_4 = \frac{11}{6} + \frac{3s}{2h_x} + \frac{w_x^2}{4h_x^2} + \frac{3\delta_x^2}{4h_x^2}$$

By using the previous expressions it is possible to write the force and the torque produced by the described actuation scheme. In particular, in the case of *force actuation* ($A_F \neq 0$ and $A_\tau = 0$) it re-

sults:

$$F_F = \frac{C_0}{h_x} A_F \left(2 + \frac{6}{h_x^2} x^2 + 2K_1 \varphi^2\right); \quad \tau_F = \frac{C_0 \delta_x}{2h_x} A_F (2y + 2\delta_x K_3 x\varphi) \tag{A.5}$$

while in case of *torque actuation* ($A_F = 0$ and $A_\tau \neq 0$) it results:

$$\tau_\tau = \frac{C_0 \delta_x}{2h_x} A_\tau \left(2 + \frac{6}{h_x^2} x^2 + 2K_4 \varphi^2\right); \quad F_\tau = \frac{C_0}{h_x} A_\tau \frac{12}{h_x^2} \varphi x$$

Finally, by defining the dimensionless crosstalks between force and torque as:

$$CT_{F\to\tau} = \frac{\tau_F}{F_F \delta_x}; \quad CT_{\tau\to F} = \frac{F_\tau \delta_x}{\tau_\tau}$$

and by retaining only terms up to the second order in $x$, $y$ and $\varphi$, they result:

$$CT_{F\to\tau} = \frac{1}{\delta_x} y + \frac{K_3}{2} x\varphi; \quad CT_{\tau\to F} = \frac{6\delta_X}{h_x^2} x\varphi \tag{A.6}$$

## References


[1] L. Carbone, et al., Phys. Rev. Lett. 91 (2003) 151101.
[2] The eLISA consortium, The gravitational universe2017. arXiv:1305.5720[astro-ph.CO] (2013) and Laser Interferometer Space Antenna, [astro-ph.IM] arXiv:1702.00786.
[3] M. Bassan, et al., Phys. Rev. Lett. 116 (2016) 051104.
[4] F. Antonucci, et al., Classical Quantum Gravity 29 (2012) 124014.
[5] M. Armano, et al., Phys. Rev. Lett. 116 (2016) 231101.
[6] R. Stanga, et al., J. Phys. Conf. Ser. 154 (2009) 012032.
[7] R. Dolesi, et al., Classical Quantum Gravity 20 (2003) S99.
[8] N. Brandt, et al., LISA technology package experiment performance budget, 2010. Issue 2.4, ESA document reference: S2-ASD-RP-3036.
[9] F. Acernese, et al., Classical Quantum Gravity 22 (2005) S279.
[10] R. De Rosa, et al., Astropart. Phys. 34 (2011) 394.
[11] L. Gan, D. Mance, P. Zweifel, Sens. Actuators A 167 (2011) 574.
[12] M. Bassan, et al., Phys. Rev. D 87 (2013) 122006.
[13] M. Bassan, et al., Phys. Lett. A 377 (2013) 1555–1660.
[14] W.J. Weber, et al., Position sensors for flight testing of LISA drag-free control, in: Proc. SPIE 4856, Gravitational-Wave Detection, 2003, pp. 31–42.
[15] M. Hueller, Geodesic motion of LISA test masses: development and testing of drag-free position sensors, University of Trento, 2003 Phd thesis.